European Journal of Mechanics B/Fluids 28 (2009) 630–640

Contents lists available at ScienceDirect

European Journal of Mechanics B/Fluids

journal homepage: www.elsevier.com/locate/ejmflu

Natural convection cooling of a localised heat source at the bottom of a nanofluid-filled enclosure

S.M. Aminossadati [a,*], B. Ghasemi [b]

[a] School of Engineering, The University of Queensland, CRCMining, Brisbane QLD 4072, Australia
[b] Faculty of Engineering, Shahrekord University P.O. Box 115, Shahrekord, Iran

ARTICLE INFO

Article history:
Received 28 January 2009
Received in revised form
10 April 2009
Accepted 25 May 2009
Available online 6 June 2009

Keywords:
Natural convection
Nanofluid
Heat source
Rayleigh number

ABSTRACT

This article presents a numerical study of natural convection cooling of a heat source embedded on the bottom wall of an enclosure filled with nanofluids. The top and vertical walls of the enclosure are maintained at a relatively low temperature. The transport equations for a Newtonian fluid are solved numerically with a finite volume approach using the SIMPLE algorithm. The influence of pertinent parameters such as Rayleigh number, location and geometry of the heat source, the type of nanofluid and solid volume fraction of nanoparticles on the cooling performance is studied. The results indicate that adding nanoparticles into pure water improves its cooling performance especially at low Rayleigh numbers. The type of nanoparticles and the length and location of the heat source proved to significantly affect the heat source maximum temperature.

1. Introduction

The heat removal strategies in many engineering applications such as cooling of electronic components rely on natural convection heat transfer due to its simplicity, minimum cost, low noise, smaller size and reliability [1]. A review of the literature indicates that natural convection in enclosures has attracted considerable interest amongst researchers in the past few decades. Many researchers have simulated the heat removal mechanism by means of natural convection in enclosures heated from below [2–5]. More recently, Cheikh et al. [6] studied natural convection in a square enclosure heated from below and cooled from above for a variety of thermal boundary conditions at the top and sidewalls. They carried out their simulation for two different lengths of the heat source and various Rayleigh numbers. They argued that the maximum temperature of the heat source did not change significantly for the diffusion dominated cases whereas decreased rather rapidly with Rayleigh number for convection dominated regimes.

In most natural convection studies, the base fluid in the enclosure has a low thermal conductivity, which limits the heat transfer enhancement. However, the continuing miniaturisation of electronic devices requires further heat transfer improvements from an energy saving viewpoint. An innovative technique, which uses a mixture of nanoparticles and the base fluid was first introduced by Choi [7] in order to develop advanced heat transfer fluids with substantially higher conductivities. The resulting mixture of the base fluid and nanoparticles having unique physical and chemical properties is referred to as a nanofluid. It is expected that the presence of the nanoparticles in the nanofluid increases the thermal conductivity and therefore substantially enhances the heat transfer characteristics of the nanofluid. Eastman et al. [8], Xie et al. [9] and Jana et al. [10] showed that higher thermal conductivity can be achieved in thermal systems utilising nanofluids. Hwang et al. [11] measured thermal conductivities of various nanofluids and showed that the thermal conductivity enhancement of nanofluids depended on the volume fraction of the suspended particles and the thermal conductivities of the particles and base fluids.

Differentially heated enclosures are extensively used to simulate natural convection heat transfer within systems using nanofluids [12–15]. Recently, Oztop and Abu-Nada [16] numerically studied heat transfer and fluid flow due to buoyancy forces in a partially heated enclosure using nanofluids made with different types of nanoparticles. They argued that the heat transfer enhancement was more pronounced at low aspect ratios than at high aspect ratios of the enclosure. They found that for all Rayleigh numbers, the mean Nusselt number increased as the volume fraction of nanoparticles increased.

* Corresponding author. Tel.: +61 7 33653676; fax: +61 7 33653888.
E-mail address: uqsamino@uq.edu.au (S.M. Aminossadati).

0997-7546/$ – see front matter © 2009 Elsevier Masson SAS. All rights reserved.
doi:10.1016/j.euromechflu.2009.05.006

Nomenclature

b	length of heat source, m
B	dimensionless length of heat source (b/L)
C_P	specific heat, J kg^{-1} K^{-1}
d	distance of heat source from the left wall, m
D	dimensionless distance of heat source from the left wall (d/L)
g	gravitational acceleration, m s^{-2}
k	thermal conductivity, W m^{-1} K^{-1}
L	cavity length, m
Nu_s	local Nusselt number on the heat source surface
Nu_m	average Nusselt number along the heat source
p	fluid pressure, Pa
$\overline{p}$	modified pressure ($p+\rho_c g y$)
P	dimensionless pressure ($\overline{p}L^2/\rho_{nf}\alpha_f^2$)
Pr	Prandtl number (ν_f/α_f)
q''	heat generation per area, W/m^2
Ra	Rayleigh number ($g\beta_f L^3\Delta T/\nu_f\alpha_f$)
T	temperature, K
u,v	velocity components in x,y directions, m s^{-1}
U,V	dimensionless velocity components ($uL/\alpha_f, vL/\alpha_f$)
x,y	Cartesian coordinates, m
X,Y	dimensionless coordinates (x/L, y/L)

Greek symbols

α	thermal diffusivity, m^2 s^{-1}($k/\rho C_p$)
β	thermal expansion coefficient, K^{-1}
ΔT	Ref. temperature difference ($q''L/k_f$)
ϕ	solid volume fraction
θ	dimensionless temperature ($T-T_c/\Delta T$)
μ	Dynamic viscosity, N s m^{-2}
ν	kinematic viscosity, m^2 s^{-1}(μ/ρ)
ρ	density, kg m^{-3}

Subscripts

c	cold wall
f	pure fluid
nf	nanofluid
p	nanoparticle
s	surface of the heat source

Contradictory results have been reported in the literature that dispersion of nanoparticles in the base fluid may result in considerable decrease in heat transfer. Putra et al. [17] and Wen and Ding [18] found a systematic and definite deterioration in the heat transfer for a particular range of Rayleigh numbers and density and concentration of nanoparticles. Similar results were also obtained by Santra et al. [19] who modelled the nanofluid as a non-Newtonian fluid. Ho et al. [20] argued that the heat transfer in a square enclosure filled nanofluids can be enhanced or mitigated depending on the formulas used for the estimated dynamic viscosity of the nanofluid. Hwang et al. [21] theoretically investigated thermal characteristics of natural convection in a rectangular cavity filled with a water-based nanofluid containing alumina. They argued that the ratio of the heat transfer coefficient of the nanofluid to that of the base fluid decreases as the size of nanoparticles increases.

Despite a number of experimental and numerical studies on natural convection in heated from below enclosures which have been reported in the literature, there is still a serious lack of information regarding the problem of heat transfer enhancement in enclosures filled with nanofluids. In fact, to the best knowledge of the authors, no studies have been reported in the literature, which investigate the natural convection cooling of a localised heat source embedded on the bottom wall of an enclosure filled with nanofluids. This problem may be encountered in a number of electronic cooling devices equipped with nanofluids. As such, the focus of the present study is on the analysis of several pertinent parameters such as Rayleigh number, length and location of the heat source and solid particles volume ratio on the natural convection characteristics within an enclosure filled with various nanofluids.

2. Problem description

Fig. 1 displays the schematic diagram of the two-dimensional enclosure considered in this study. A heat source is located on the bottom wall of the enclosure which is thermally insulated. The vertical walls and the horizontal top wall of the enclosure are maintained at a relatively low temperature (T_c). The nanofluids used in the analysis are assumed to be Newtonian, incompressible and laminar. The base fluid (water) and the solid spherical nanoparticles (Cu, Ag, Al_2O_3 and TiO_2) are in thermal equilibrium. The thermo-physical properties of the base fluid and the nanoparticles are given in Table 1 [22]. The thermo-physical properties of the nanofluid are assumed constant except for the density variation, which is determined based on the Boussinesq approximation.

3. Mathematical formulation

The continuity, momentum and energy equations for the laminar and steady state natural convection in the two-dimensional enclosure can be written in dimensional form as follows:

$$\frac{\partial u}{\partial x}+\frac{\partial v}{\partial y}=0 \tag{1}$$

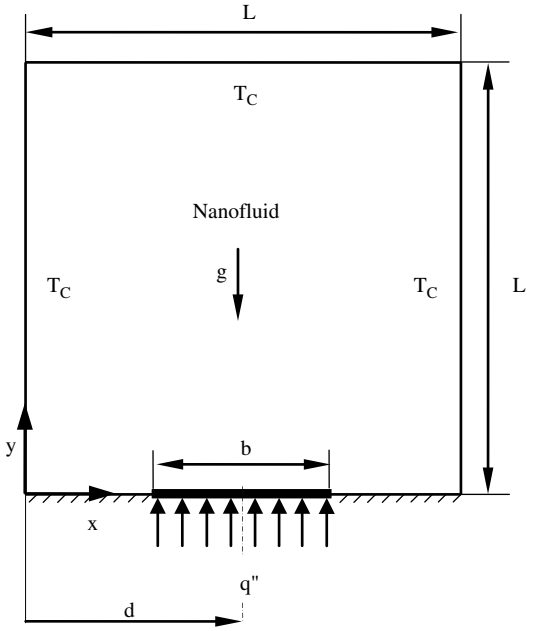

Fig. 1. A schematic diagram of the physical model.

Table 1
Thermo-physical properties of water and nanoparticles [22].

	ρ (kg m^{-3})	C_P (J kg^{-1} K^{-1})	k (W m^{-1} K^{-1})	$\beta \times 10^5$ (K^{-1})
Pure Water	997.1	4179	0.613	21
Copper (Cu)	8933	385	401	1.67
Silver (Ag)	10,500	235	429	1.89
Alumina (Al_2O_3)	3970	765	40	0.85
Titanium Oxide (TiO_2)	4250	686.2	8.9538	0.9

$$u\frac{\partial u}{\partial x}+v\frac{\partial u}{\partial y}=\frac{1}{\rho_{nf}}\left[-\frac{\partial p}{\partial x}+\mu_{nf}\left(\frac{\partial^2 u}{\partial x^2}+\frac{\partial^2 u}{\partial y^2}\right)\right] \tag{2}$$

$$u\frac{\partial v}{\partial x}+v\frac{\partial v}{\partial y}=\frac{1}{\rho_{nf}}\left[-\frac{\partial p}{\partial y}+\mu_{nf}\left(\frac{\partial^2 v}{\partial x^2}+\frac{\partial^2 v}{\partial y^2}\right)+(\rho\beta)_{nf}g(T-T_c)\right] \tag{3}$$

$$u\frac{\partial T}{\partial x}+v\frac{\partial T}{\partial y}=\alpha_{nf}\left(\frac{\partial^2 T}{\partial x^2}+\frac{\partial^2 T}{\partial y^2}\right) \tag{4}$$

where, the effective density of the nanofluid is given as

$$\rho_{nf}=(1-\phi)\rho_f+\phi\rho_p, \tag{5}$$

and ϕ is the solid volume fraction of nanoparticles. Thermal diffusivity of the nanofluid is:

$$\alpha_{nf}=k_{nf}/(\rho C_p)_{nf} \tag{6}$$

where, the heat capacitance of the nanofluid given is:

$$(\rho C_p)_{nf}=(1-\phi)(\rho C_p)_f+\phi(\rho C_p)_p. \tag{7}$$

The thermal expansion coefficient of the nanofluid can be determined by

$$(\rho\beta)_{nf}=(1-\phi)(\rho\beta)_f+\phi(\rho\beta)_p, \tag{8}$$

The effective dynamic viscosity of the nanofluid given by Brinkman [23] is:

$$\mu_{nf}=\frac{\mu_f}{(1-\phi)^{2.5}} \tag{9}$$

In Equation (6), k_{nf} is the thermal conductivity of the nanofluid, which for spherical nanoparticles, according to Maxwell [24], is:

$$k_{nf}=k_f\left[\frac{(k_p+2k_f)-2\phi(k_f-k_p)}{(k_p+2k_f)+\phi(k_f-k_p)}\right] \tag{10}$$

where, k_p is the thermal conductivity of dispersed nanoparticles and k_f is the thermal conductivity of pure fluid. This classical model has been sited by other researchers such as Ho et al. [20] and Oztop and Abu-Nada [16].

Equations (1)–(4) can be converted to non-dimensional forms, using the following non-dimensional parameters:

Table 2
Grid independency results (Water–Cu, $B=0.4$, $D=0.5$, $\phi=0.1$, Ra $=10^5$).

Grid	20×20	40×40	60×60	80×80	100×100
Nu_m	7.2057	7.1284	7.1214	7.1209	7.1209
$\theta_{s,max}$	0.1689	0.1719	0.1723	0.1725	0.1725

Table 3
Validation of the present code against case C1 in Cheikh et al. [6].

			Rayleigh Number				
			10^3	10^4	10^5	10^6	10^7
$B=0.2$	Nu_m	Present work	5.9228	5.9539	7.5910	12.0624	20.0195
		Cheikh et al. [6]	5.9152	5.9467	7.5805	12.0390	19.9801
		Error (%)	0.13	0.12	0.14	0.19	0.19
	T_{max}	Present work	0.1819	0.1815	0.1484	0.1040	0.0729
		Cheikh et al. [6]	0.1819	0.1815	0.1484	0.1040	0.0730
		Error (%)	0	0	0	0	0.14
$B=0.8$	Nu_m	Present work	3.5551	3.8060	6.2944	9.9159	16.6779
		Cheikh et al. [6]	3.5532	3.8047	6.2942	9.9160	16.7432
		Error (%)	0.05	0.05	0	0	0.4
	T_{max}	Present work	0.3642	0.3636	0.2495	0.1700	0.1160
		Cheikh et al. [6]	0.3642	0.3635	0.2494	0.1701	0.1163
		Error (%)	0	0.03	0.04	0.06	0.26

$$X=\frac{x}{L},\quad Y=\frac{y}{L},\quad U=\frac{uL}{\alpha_f},\quad V=\frac{vL}{\alpha_f},\quad P=\frac{\bar{p}L^2}{\rho_{nf}\alpha_f^2}$$
$$\theta=\frac{T-T_c}{\Delta T},\quad \mathrm{Ra}=\frac{g\beta_f L^3\Delta T}{\nu_f\alpha_f},\quad \Delta T=\frac{q''L}{k_f},\quad \mathrm{Pr}=\frac{\nu_f}{\alpha_f} \tag{11}$$

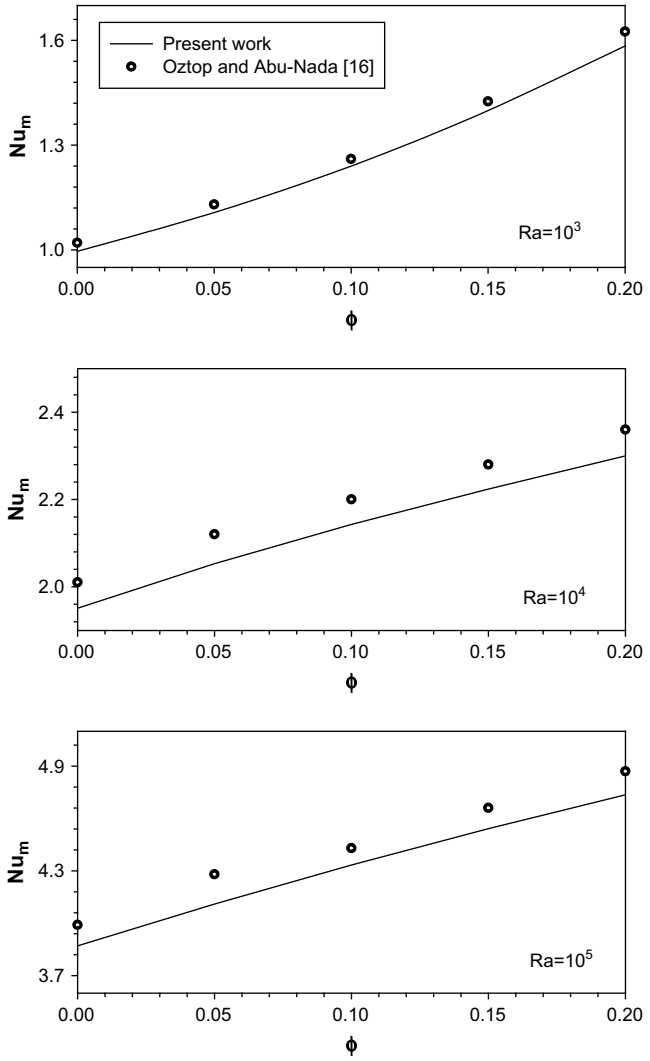

Fig. 2. Validation of the present code for Cu–water nanofluid against Oztop and Abu-Nada [16].

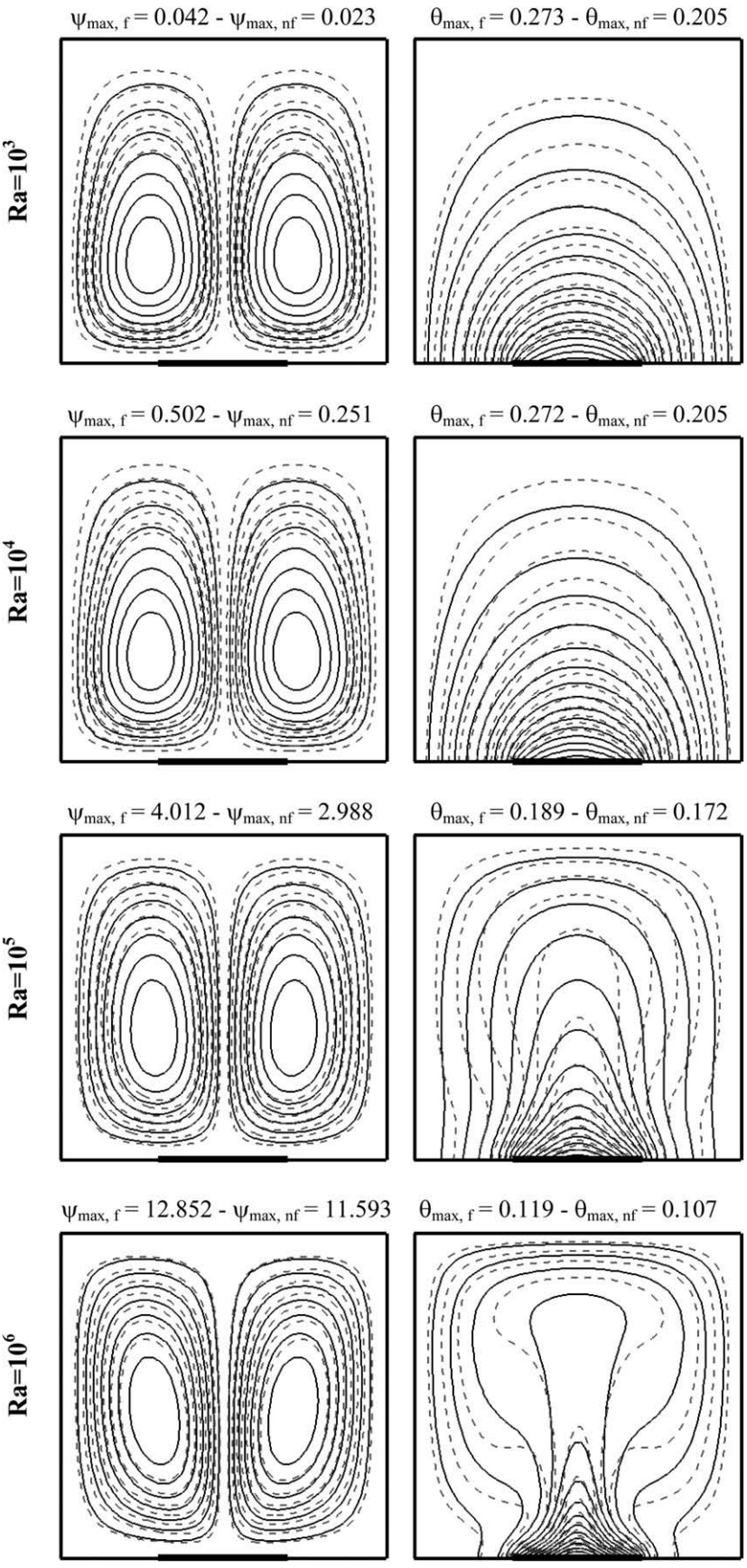

Fig. 3. Streamlines (left) and isotherms (right) for the enclosures filled with Cu–water nanofluid, $\phi = 0.1$, (—) and pure water (- - - -) at different Rayleigh numbers ($D = 0.5$ and $B = 0.4$).

The non-dimensional continuity, momentum and energy equations are written as follows:

$$\frac{\partial U}{\partial X}+\frac{\partial V}{\partial Y}=0 \tag{12}$$

$$U\frac{\partial U}{\partial X}+V\frac{\partial U}{\partial Y}=-\frac{\partial P}{\partial X}+\frac{\mu_{nf}}{\rho_{nf}\alpha_f}\left(\frac{\partial^2 U}{\partial X^2}+\frac{\partial^2 U}{\partial Y^2}\right) \tag{13}$$

$$U\frac{\partial V}{\partial X}+V\frac{\partial V}{\partial Y}=-\frac{\partial P}{\partial Y}+\frac{\mu_{nf}}{\rho_{nf}\alpha_f}\left(\frac{\partial^2 V}{\partial X^2}+\frac{\partial^2 V}{\partial Y^2}\right)+\frac{(\rho\beta)_{nf}}{\rho_{nf}\beta_f}\,\mathrm{Ra}\,\mathrm{Pr}\,\theta \tag{14}$$

$$U\frac{\partial \theta}{\partial X}+V\frac{\partial \theta}{\partial Y}=\frac{\alpha_{nf}}{\alpha_f}\left(\frac{\partial^2 \theta}{\partial X^2}+\frac{\partial^2 \theta}{\partial Y^2}\right) \tag{15}$$

The boundary conditions, used to solve the equations (12)–(15) are as follows:

$$\begin{aligned}
&U=V=0 \text{ and } \theta=0 \quad \text{for } X=0 \text{ and } 0\le Y\le 1\\
&U=V=0 \text{ and } \theta=0 \quad \text{for } X=1 \text{ and } 0\le Y\le 1\\
&U=V=0 \text{ and } \frac{\partial\theta}{\partial Y}=0 \quad \text{for } Y=0 \text{ and } 0\le X<(D-0.5B)\\
&U=V=0 \text{ and } \frac{\partial\theta}{\partial Y}=-\frac{k_f}{k_{nf}} \quad \text{for } Y=0 \text{ and}\\
&\quad (D-0.5B)\le X\le (D+0.5B)\\
&U=V=0 \text{ and } \frac{\partial\theta}{\partial Y}=0 \quad \text{for } Y=0 \text{ and } (D+0.5B)<X\le 1\\
&U=V=0 \text{ and } \theta=0 \quad \text{for } Y=1 \text{ and } 0\le X\le 1
\end{aligned} \tag{16}$$

The local Nusselt number on the heat source surface can be defined as:

$$\mathrm{Nu}_s=\frac{hL}{k_f} \tag{17}$$

where, h is the convection heat transfer coefficient:

$$h=\frac{q''}{T_s-T_c} \tag{18}$$

Rearranging the local Nusselt number by using the dimensionless parameters (Eq. (11)) yields:

$$\mathrm{Nu}_s(X)=\frac{1}{\theta_s(X)} \tag{19}$$

where, θ_s is the dimensionless heat source temperature. The average Nusselt number (Nu_m) is determined by integrating Nu_s along the heat source.

$$\mathrm{Nu}_m=\frac{1}{B}\int_{D-0.5B}^{D+0.5B}\mathrm{Nu}_s(X)dX \tag{20}$$

4. Numerical approach and validation

The non-dimensional governing equations along with the boundary conditions were discretised using a control volume formulation given by Patankar [25]. The SIMPLE algorithm was utilised to handle the pressure-velocity coupling. The convection-diffusion terms were treated with a power-law scheme. The numerical method was implemented in a FORTRAN program. The effect of grid resolution was examined in order to select the appropriate grid density. Table 2 presents the results of a grid independency study showing the effects of number of grid points on Nu_m and $\theta_{s,max}$ respectively for five different mesh combinations (Cu–water, $B=0.4$, $D=0.5$, $\phi=0.1$, $\mathrm{Ra}=10^5$). A 60×60 uniform grid is found to meet the requirements of both the grid independency study and the computational time limits. The convergence

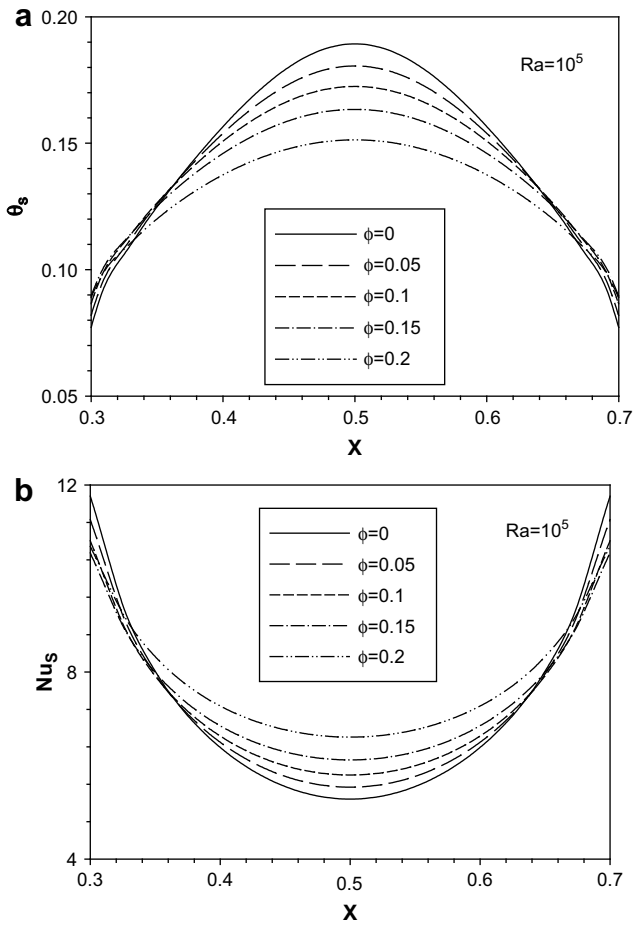

Fig. 4. a) Profile of local temperature along the heat source for various solid volume fractions (Cu–Water, $\mathrm{Ra}=10^5$, $D=0.5$ and $B=0.4$), b) Profile of local Nusselt number along the heat source for various solid volume fractions (Cu–Water, $\mathrm{Ra}=10^5$, $D=0.5$ and $B=0.4$).

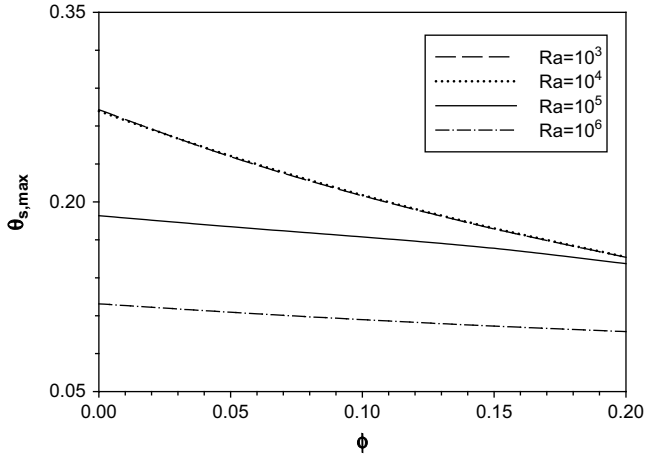

Fig. 5. Variation of heat source maximum temperature with solid volume fraction at various Rayleigh numbers (Cu–Water, $D=0.5$ and $B=0.4$).

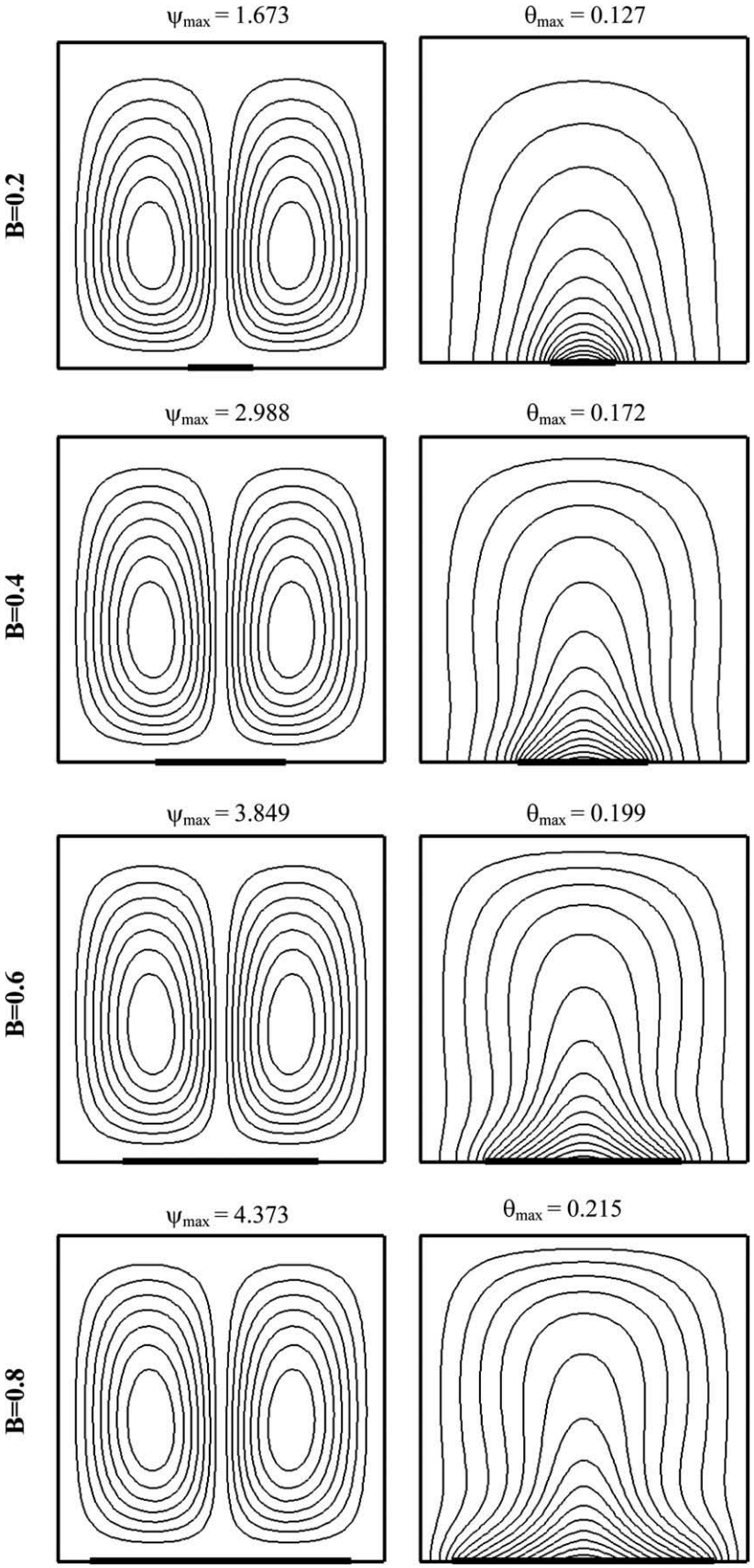

Fig. 6. Streamlines (left) and isotherms (right) for the enclosures filled with Cu–water nanofluid for different heat source lengths ($Ra = 10^5$, $\phi = 0.1$ and $D = 0.5$).

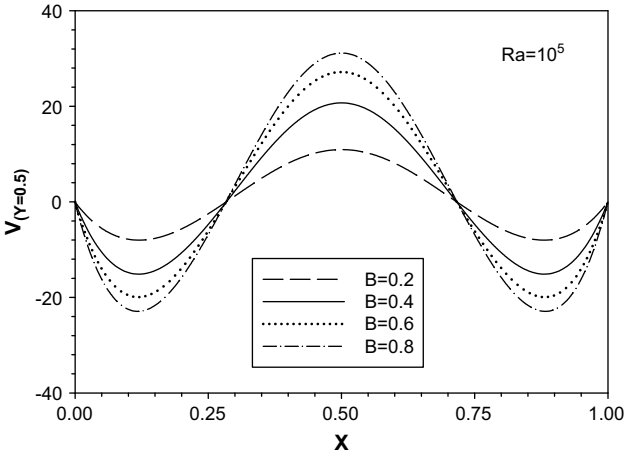

Fig. 7. Vertical velocity profiles along the mid-section of the enclosure for various heat source lengths (Cu–Water, $Ra = 10^5$, $D = 0.5$ and $\phi = 0.1$).

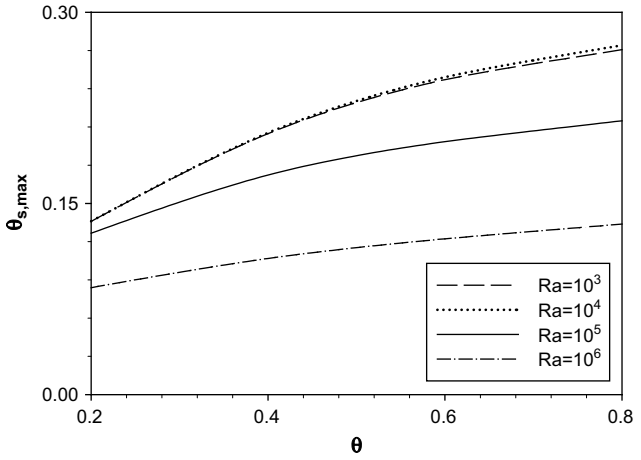

Fig. 9. Variation of heat source maximum temperature with heat source length at various Rayleigh numbers (Cu–Water, $D = 0.5$ and $\phi = 0.1$).

criteria was to reduce the maximum mass residual of the grid control volume below 10^{-9}.

The present numerical code was validated against the results of other natural convection studies in enclosures developed by De Vahl Davis [26] and Cheikh et al. [6]. Table 3 compares the results of the present simulation with the study by Cheikh et al. [6] in terms of the values of Nu_m and T_{max} at various Rayleigh numbers and two different heat source lengths. Finally, the present code was further validated against the study by Oztop and Abu-Nada [16] for natural convection in a partially heated enclosure filled with Cu–water nanofluid at different Rayleigh numbers (Fig. 2).

5. Results

The cooling performance of the nanofluid-filled enclosure is studied for a range of solid volume fractions ($0 \le \phi \le 0.2$), heat source lengths ($0.2 \le B \le 0.8$), heat source locations ($0.2 \le D \le 0.5$) and a choice of nanoparticles (Cu, Ag, Al_2O_3 and TiO_2). For all simulations, pure water is considered as the base fluid with $Pr = 6.2$.

5.1. The effects of solid volume fraction

In this part of the study, an enclosure filled with Cu–water nanofluid with a heat source ($B = 0.4$) located in the middle of the bottom wall ($D = 0.5$) is considered.

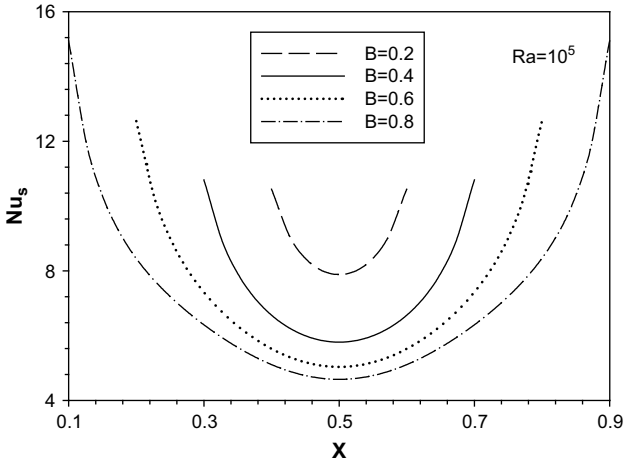

Fig. 8. Profile of local Nusselt number along the heat source for various heat source lengths (Cu–Water, $Ra = 10^5$, $D = 0.5$ and $\phi = 0.1$).

Fig. 3 presents the streamlines (left) and isotherms (right) for the nanofluid, $\phi = 0.1$, (—) and pure water (- - - -) at different Rayleigh numbers. Since the heat source is located in the middle of the bottom wall, symmetrical flow and temperature patterns are observed in the enclosure. The streamlines show two counter-rotating circulating cells for all values of Rayleigh number. In fact, the buoyant forces generated due to the fluid temperature differences cause the fluid to rise in the middle and to descend on the sides of the enclosure. This movement of the fluid forms counter-rotating circulating cells within the enclosure. It can be observed that even though the shape of the circulating cells do not change with Ra, their intensity increases as the buoyant forces become stronger. It must be noted that the contact line of the symmetrical circulation zones agrees with the axis of symmetry of the heat source for all Rayleigh numbers.

The isotherms also have symmetrical shape at each Ra, however, they display different behaviours as Rayleigh number changes. For the cases of $Ra = 10^3$ and 10^4, where conduction dominates the flow regime, the isotherms are distributed near the heat source and tend to be parallel to the heat source. As the Rayleigh number increases, streamlines exhibit stronger flow patterns and isotherms display more distinguished boundary layers. It is clear that the flow and temperature patterns are influenced by the presence of nanoparticles. That is to say, the addition of nanoparticles to pure water reduces the strength of flow field as observed by other researchers such as Ho et al. [20]. This reduction is more pronounced at low Rayleigh numbers where conduction heat transfer dominates. It is also apparent that as nanoparticles are added, the maximum dimensionless temperature is reduced which is an indication of enhancing the enclosure cooling performance.

The surface temperature of heated surfaces such as electronic components with fixed heat flux is not uniform and has a maximum value where the temperature difference with the adjacent flow is minimal (Fig. 4a). At this point, for all solid volume fractions, the corresponding Nusselt number is minimum (Fig. 4b). The uncontrolled surface temperature of electronic components is detrimental to their life and functionality. Fig. 5 shows that the maximum surface temperature of the heat source is reduced by increasing the solid volume fraction of nanoparticles. This reduction is less evident as the heat transfer mechanism within the enclosure shifts from conduction (low Rayleigh numbers) to convection (high Rayleigh numbers) dominated flow.

It is noted that the reduction in the heat source maximum temperature is a result of the enhancement in the heat removal

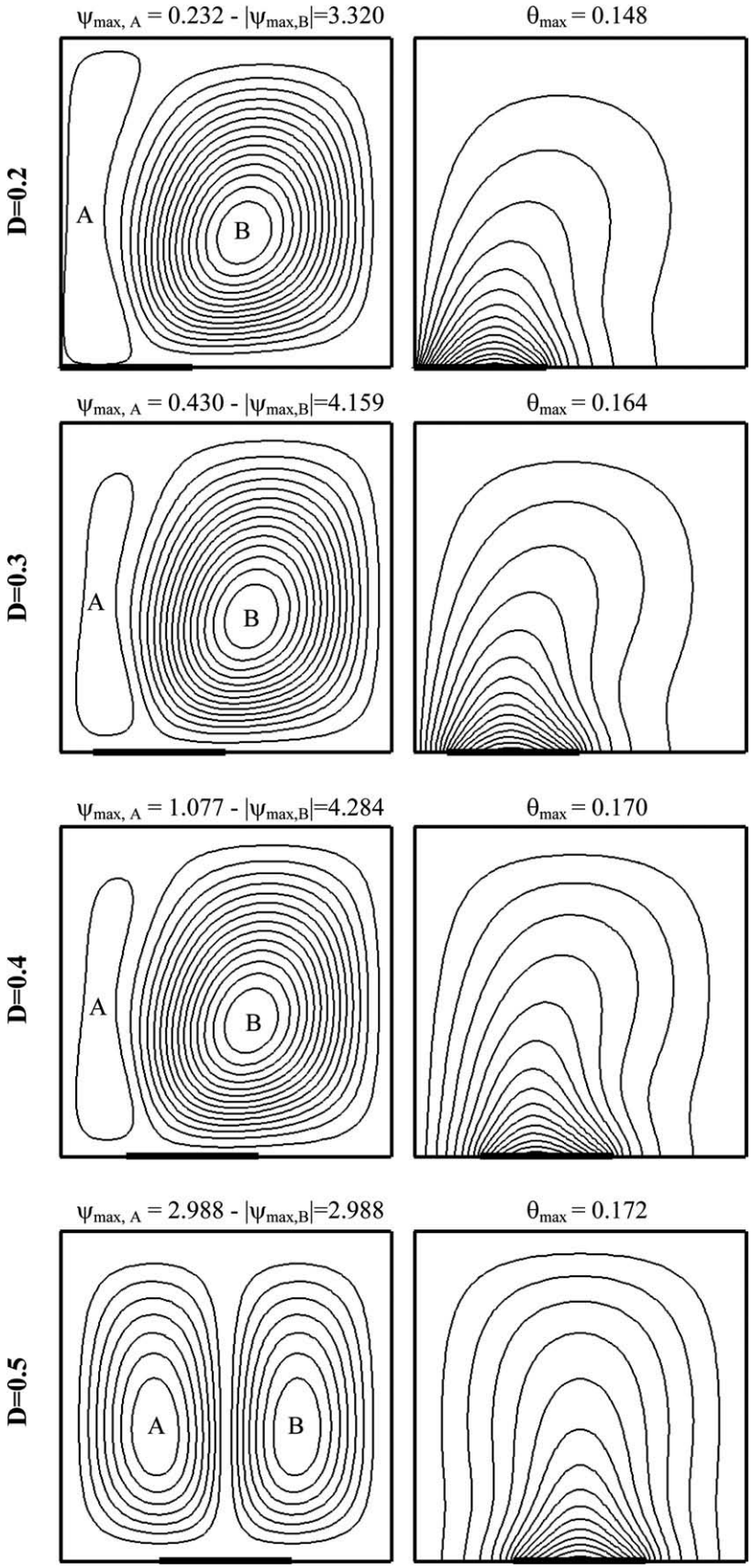

Fig. 10. Streamlines (left) and isotherms (right) for the enclosures filled with Cu–water nanofluid for different locations of the heat source ($Ra = 10^5$, $\phi = 0.1$ and $B = 0.4$).

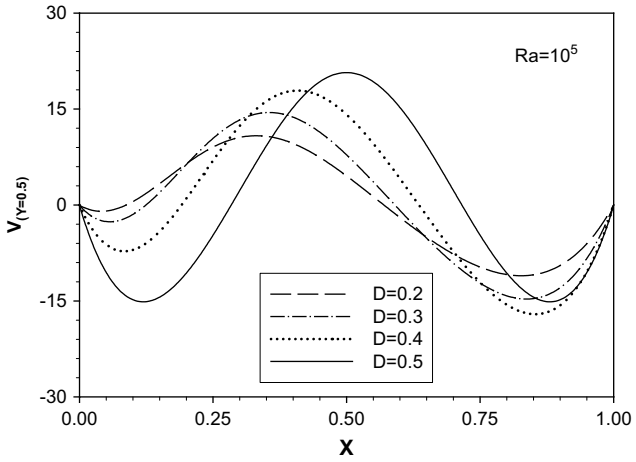

Fig. 11. Vertical velocity profiles along the mid-section of the enclosure for different locations of the heat source (Cu–Water, $Ra = 10^5$, $B = 0.4$ and $\phi = 0.1$).

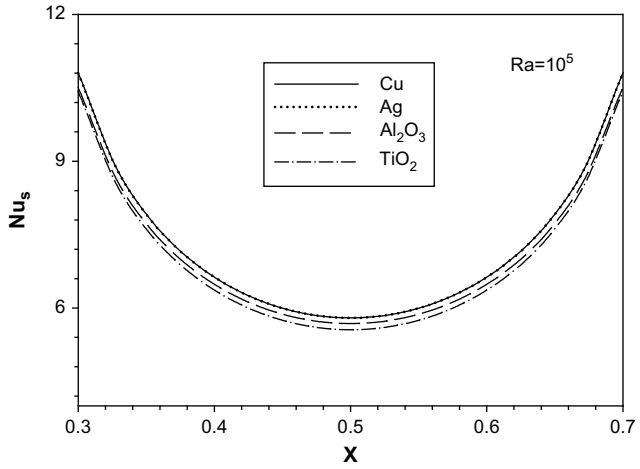

Fig. 13. Profile of local Nusselt number along the heat source for different types of nanofluids ($Ra = 10^5$, $B = 0.4$, $D = 0.5$ and $\phi = 0.1$).

process, which is in turn due to the addition of nanoparticles with a higher thermal conductivity than the base fluid. However, since the addition of nanoparticles improves the effective thermal conductivity of the nanofluid, the reduction of the heat source maximum temperature is more noticeable for situations where conduction dominates the heat transfer mechanism.

5.2. The effects of heat source length

In this part of the study, an enclosure filled with Cu–water nanofluid ($\phi = 0.1$) with a heat source located in the middle of the bottom wall ($D = 0.5$) is considered.

Fig. 6 shows the effects of heat source lengths on the streamlines (left) and the isotherms (right) at $Ra = 10^5$. The figures show that as the heat source length increases, the two counter-rotating rotation cells within the enclosure are intensified and higher temperature patterns are observed. This can be explained by higher heat generation rates as the heat source length increases. Moreover, higher heat generation rates are associated with stronger buoyant forces which intensify the circulating cells. It is also noted that since the heat source remains in the middle of the bottom wall, symmetrical circulating cells are generated regardless of the length of the heat source.

In order to have a better understanding of the flow behaviour in this situation, the vertical velocity profiles along the mid-section of the enclosure are presented in Fig. 7. Symmetrical velocity profiles are observed which indicate the direction of the flow rotation

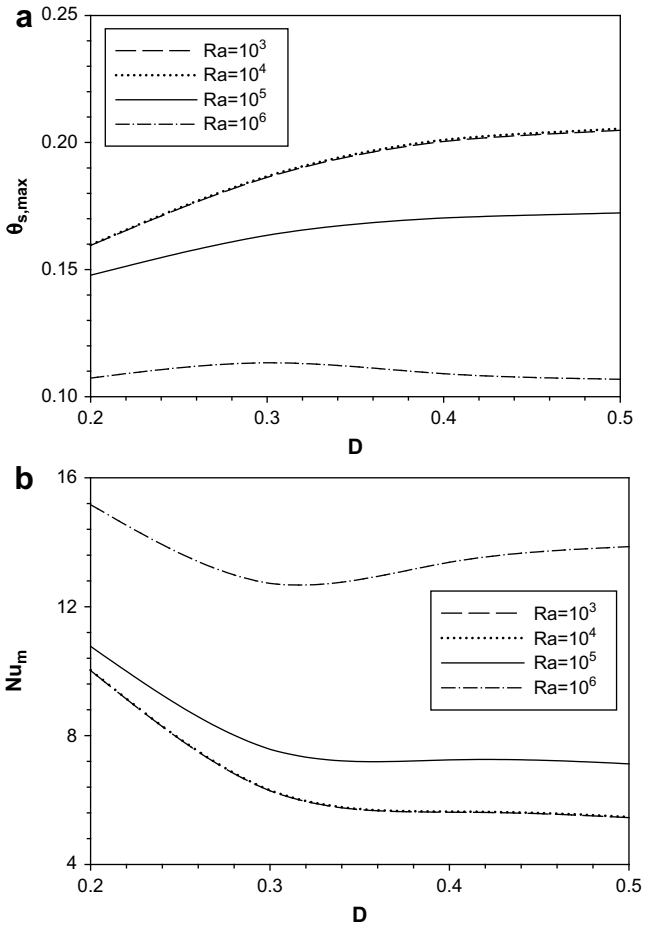

Fig. 12. a) Variation of heat source maximum temperature with heat source location at various Rayleigh numbers (Cu–Water, $B = 0.4$ and $\phi = 0.1$), b) Variation of average Nusselt number with heat source location at various Rayleigh numbers (Cu–Water, $B = 0.4$ and $\phi = 0.1$).

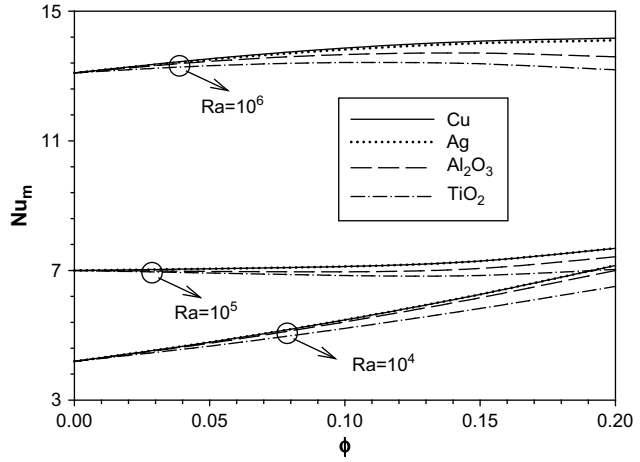

Fig. 14. Variation of average Nusselt number with solid volume fraction at various Rayleigh numbers for different nanofluids ($D = 0.5$, $B = 0.4$).

Table 4
Benchmark results for the base case ($\phi = 0.1$, $B = 0.4$, $D = 0.5$).

		Nu_m	$\theta_{s,max}$	$\lvert\psi_{max}\rvert$
$Ra = 10^3$	Cu	5.451	0.205	0.023
	Ag	5.451	0.205	0.024
	Al_2O_3	5.391	0.207	0.022
	TiO_2	5.189	0.215	0.023
$Ra = 10^4$	Cu	5.474	0.205	0.251
	Ag	5.474	0.205	0.257
	Al_2O_3	5.411	0.208	0.238
	TiO_2	5.212	0.216	0.250
$Ra = 10^5$	Cu	7.121	0.172	2.988
	Ag	7.119	0.172	3.061
	Al_2O_3	6.956	0.176	2.875
	TiO_2	6.842	0.180	2.948
$Ra = 10^6$	Cu	13.864	0.107	11.593
	Ag	13.816	0.107	11.901
	Al_2O_3	13.663	0.108	11.260
	TiO_2	13.416	0.111	11.277

within the enclosure. In fact, the flow rises in the middle and descends near the vertical walls. It is also clear that the absolute magnitude of vertical velocity increases with increasing the heat source length. This is because of stronger buoyant flow for higher heat generation rates.

Fig. 8 shows symmetrical profiles of the local Nusselt number along the heat source for different heat source lengths. As stated earlier, the highest and the lowest local Nusselt number are obtained at both ends and at the middle of the heat source, respectively. In general, increasing the heat source length causes the local Nusselt number profile to decrease. By considering Equation (19), the inverse of this trend can be predicted for the heat source temperature profile.

The effects of heat source length on the enclosure cooling performance can be more clearly understood from Fig. 9, where the heat source maximum temperature is plotted for a range of Rayleigh numbers. It can be seen that in the convection dominated flow regime, the maximum temperature decreases as Rayleigh number increases due to stronger buoyancy forces. As the length of the heat source increases, the maximum temperature continuously increases due to the higher heat flux generated by the heat source.

5.3. The effects of heat source location

In this part of the study, an enclosure filled with Cu–water nanofluid ($\phi = 0.1$) with a heat source ($B = 0.4$) is considered.

Fig. 10 displays the streamlines (left) and the isotherms (right) for different locations of the heat source on the bottom wall at $Ra = 10^5$. Two unsymmetrical circulating cells with unequal strengths are observed when the heat source is located next to the left wall. As the heat source moves away from the left wall, the strength of both circulating cells increases until it reaches the middle of the bottom wall, where two circulating cells with equal intensity appear in the enclosure. The isotherms show that as the heat source moves away from the left cold wall, the maximum flow temperature increases. This can be explained by the distance that the fluid needs to travel in the circulating cell to exchange the heat between the heat source and the left cold wall. In fact, the closer the heat source is to the left cold wall, the higher heat removal and the lower heat source maximum temperature is achieved. It is clear that the isotherms follow the movement of the heat source and their extension in the enclosure becomes more noticeable as the heat source moves away from the left wall.

Fig. 11 presents the vertical velocity profiles along the mid-section of the enclosure. The results prove the existence of two counter-rotating circulating cells for all different locations of the heat source. For the cases, where the heat source is not located in the middle, unsymmetrical velocity profiles indicate unbalanced circulating cells within the enclosure. Moreover, the maximum velocity increases as the heat source moves towards the middle.

Fig. 12a and b presents the effects of the location of heat source on its maximum temperature and average Nusselt number, respectively. At low Rayleigh numbers, as the heat source moves towards the middle of the bottom wall, the maximum temperature increases and the corresponding average Nusselt number decreases. This is because of moving the heat source away from the cold wall. On the contrary, at high Rayleigh numbers ($Ra = 10^6$), the heat source temperature reaches its maximum and the corresponding average Nusselt number reaches its minimum at $D = 0.3$. This behaviour can be related to the stronger buoyant flows at this Rayleigh number.

5.4. The effects of type of nanofluid

In this part of the study, an enclosure filled with different types of nanofluids with a heat source ($B = 0.4$ and $D = 0.5$) is considered.

Fig. 13 shows the profile of local Nusselt number along the heat source for different types of nanofluids. Symmetrical profiles are obtained for all nanofluids with the lowest Nusselt number for the middle of the heat source. Table 1 shows that TiO_2 has the lowest value of thermal conductivity compared to other nanoparticles, hence, it has the lowest values of Nusselt number. Cu and Ag, on the other hand, have the highest values. In addition, the thermal conductivity of Al_2O_3 is approximately one tenth of Cu and Ag (Table 1), thus, the Nusselt number for Al_2O_3 is lower than that for Cu and Ag.

Fig. 14 presents the variation of average Nusselt number with solid volume fraction. The figure shows that at low Rayleigh numbers ($Ra = 10^4$), the average Nusselt number increases almost monotonically with solid volume fraction for all nanofluids. It must be noted that since the results for $Ra = 10^3$ and 10^4 are almost the same, the results are only presented for $Ra = 10^4$. At $Ra = 10^5$, the average Nusselt number also increases with solid volume fraction with a lower gradient compared to that for $Ra = 10^4$. At $Ra = 10^6$, a slight increase is observed for the Nusselt number with the solid volume fraction for Cu and Ag nanoparticles, whereas, for Al_2O_3 and TiO_2, optimum values can be found for solid volume fraction which result in the highest cooling performance.

Table 4 presents some benchmark results on the steady natural convection cooling of a localised heat source at the bottom of

Table 5
The percentages of heat source maximum temperature reduction for different nanofluids respect to pure water at different Rayleigh numbers and solid volume fractions.

		$Ra = 10^3$	$Ra = 10^4$	$Ra = 10^5$	$Ra = 10^6$
$\phi = 0.05$	Cu	13.63	13.06	4.60	5.53
	Ag	13.63	13.06	4.60	5.45
	Al_2O_3	13.12	12.54	3.65	4.95
	TiO_2	11.40	10.85	2.59	3.77
$\phi = 0.10$	Cu	24.95	24.43	8.88	10.48
	Ag	24.95	24.43	8.88	10.23
	Al_2O_3	24.11	23.58	7.03	9.22
	TiO_2	21.18	20.60	4.92	7.04
$\phi = 0.15$	Cu	34.55	34.14	13.64	14.75
	Ag	34.55	34.14	13.64	14.42
	Al_2O_3	33.49	33.04	11.21	12.66
	TiO_2	29.68	29.18	7.83	9.64
$\phi = 0.20$	Cu	42.80	42.46	20.04	18.36
	Ag	42.80	42.46	20.04	18.11
	Al_2O_3	41.55	41.21	17.56	15.34
	TiO_2	37.08	36.72	12.43	11.65

a nanofluid-filled enclosure. In this Table, the values of $|\psi_{max}|$, Nu_m and $\theta_{s,max}$ are presented for $D = 0.5$, $B = 0.4$ and $\phi = 0.1$. The results confirm that as Ra increases, the buoyant flows become stronger. This in turn results in higher values for $|\psi_{max}|$ and Nu_m and lower values for $\theta_{s,max}$.

As mentioned earlier, the maximum surface temperature of the heat source is an important parameter in the thermal design of the electronic devices. In order to clarify the effects of the addition of nanoparticles on the reduction of this important parameter, Table 5 is presented. This table displays the percentages of maximum temperature reduction of the heat source for different nanofluids respect to pure water. It is evident that at low Rayleigh numbers, where the heat transfer is mainly due to conduction, the effect of adding the nanoparticles is more noticeable than that at high Rayleigh numbers. In general, amongst all nanoparticles, Cu provides the highest temperature reduction (i.e. 42.80% for $Ra = 10^3$ and $\phi = 0.20$) and TiO_2 provides the lowest temperature reduction (i.e. 2.59% for $Ra = 10^5$ and $\phi = 0.05$).

6. Conclusions

Natural convection in a partially heated enclosure from below and filled with different types of nanofluids has been numerically investigated. The effects on the enclosure cooling performance of Rayleigh number, solid volume fraction, heat source length and location and the type of nanofluid are studied. The important concluding remarks are presented below:

- The increase of Rayleigh numbers strengthens the natural convection flows which results in the reduction of heat source temperature.
- The increase of solid volume fraction of nanoparticles causes the heat source maximum temperature to decrease particularly at low Rayleigh numbers where conduction is the main heat transfer mechanism.
- The increase of heat source length increases the heat transfer to the nanofluid and therefore, increases the surface temperature of the heat source and the strength of natural convection circulating cells within the enclosure.
- As the heat source moves from the left wall towards the middle of the bottom wall of the enclosure, at low Rayleigh numbers, the heat source maximum temperature continuously increases. However, at high Rayleigh numbers, a critical location ($D = 0.3$) is found which is associated with the highest heat source maximum temperature.
- Cu and Ag nanoparticles proved to have the highest cooling performance such that at low Rayleigh numbers, the addition of 20% of these nanoparticles to pure water results in 42.8% reduction of heat source maximum temperature.
- Even though, the addition of Al_2O_3 and TiO_2 also reduces the heat source maximum temperature, their influence is not as significant as that for Cu and Ag nanoparticles.

References

[1] S. Ostrach, Natural convection in enclosures, J. Heat Transf. 110 (1988) 1175–1190.
[2] M.M. Ganzarolli, L.F. Milanez, Natural convection in rectangular enclosures heated from below and symmetrically cooled from the sides, Int. J. Heat Mass Transf. 38 (1995) 1063–1073.
[3] I. Sezai, A.A. Mohamad, Natural convection from a discrete heat source on the bottom of a horizontal enclosure, Int. J. Heat Mass Transf. 43 (2000) 2257–2266.
[4] M. Corcione, Effects of the thermal boundary conditions at the sidewalls upon natural convection in rectangular enclosures heated from bellow and cooled from above, Int. J. Therm. Sci. 42 (2003) 199–208.
[5] B. Calgagni, F. Marsili, M. Paroncini, Natural convective heat transfer in square enclosures heated from below, Appl. Therm. Eng. 25 (2005) 2522–2531.
[6] N.B. Cheikh, B.B. Beya, T. Lili, Influence of thermal boundary conditions on natural convection in a square enclosure partially heated from below, Int. Comm. Heat Mass Transf. 34 (2007) 369–379.
[7] S.U.S. Choi, Enhancing thermal conductivity of fluids with nanoparticles, ASME Fluids Eng. Division 231 (1995) 99–105.
[8] J.A. Eastman, S.U.S. Choi, S. Li, W. Yu, L.J. Thompson, Anomalously increased effective thermal conductivities of ethylene glycol-based nanofluids containing copper nanoparticles, Appl. Phys. Lett. 78 (6) (2001) 718–720.
[9] H.Q. Xie, H. Lee, W. Youn, M. Choi, Nanofluids containing multiwalled carbon nanotubes and their enhanced thermal conductivities, J. Appl. Phys. 94 (8) (2003) 4967–4971.
[10] S. Jana, A. Salehi-Khojin, W.H. Zhong, Enhancement of fluid thermal conductivity by the addition of single and hybrid nano-additives, Thermochimica Acta 462 (1–2) (2007) 45–55.
[11] Y. Hwang, J.K. Lee, C.H. Lee, Y.M. Jung, S.I. Cheong, C.G. Lee, B.C. Ku, S.P. Jang, Stability and thermal conductivity characteristics of nanofluids, Thermochimica Acta 455 (1–2) (2007) 70–74.
[12] K. Khanafer, K. Vafai, M. Lightstone, Buoyancy-driven heat transfer enhancement in a two-dimensional enclosure utilizing nanofluids, Int. J. Heat Mass Transf. 46 (19) (2003) 3639–3653.
[13] R.Y. Jou, S.C. Tzeng, Numerical research of nature convective heat transfer enhancement filled with nanofluids in rectangular enclosures, Int. Comm. Heat Mass Transf. 33 (6) (2006) 727–736.
[14] G. Polidori, S. Fohanno, C.T. Nguyen, A note on heat transfer modelling of Newtonian nanofluids in laminar free convection, Int. J. Therm. Sci. 46 (8) (2007) 739–744.
[15] A.G.A. Nnanna, Experimental model of temperature-driven nanofluid, J. Heat Transf. 129 (6) (2007) 697–704.
[16] H.F. Oztop, E. Abu-Nada, Numerical study of natural convection in partially heated rectangular enclosures filled with nanofluids, Int. J. Heat Fluid Flow 29 (5) (2008) 1326–1336.
[17] N. Putra, W. Roetzel, S.K. Das, Natural convection of nano-fluids, Heat Mass Transf. 39 (8–9) (2003) 775–784.
[18] D. Wen, Y. Ding, Formulation of nanofluids for natural convective heat transfer applications, Int. J. Heat Fluid Flow 26 (6) (2005) 855–864.
[19] A.K. Santra, S. Sen, N. Chakraborty, Study of heat transfer characteristics of copper-water nanofluid in a differentially heated square cavity with different viscosity models, J. Enhanced Heat Transf. 15 (4) (2008) 273–287.
[20] C.J. Ho, M.W. Chen, Z.W. Li, Numerical simulation of natural convection of nanofluid in a square enclosure: effects due to uncertainties of viscosity and thermal conductivity, Int. J. Heat Mass Transf. 51 (17–18) (2008) 4506–4516.
[21] K.S. Hwang, J.H. Lee, S.P. Jang, Buoyancy-driven heat transfer of water-based Al2O3 nanofluids in a rectangular cavity, Int. J. Heat Mass Transf. 50 (19–20) (2007) 4003–4010.
[22] E. Abu-Nada, Z. Masoud, A. Hijazi, Natural convection heat transfer enhancement in horizontal concentric annuli using nanofluids, Int. Comm. Heat Mass Transf. 35 (5) (2008) 657–665.
[23] H.C. Brinkman, The viscosity of concentrated suspensions and solution, J. Chem. Phys. 20 (1952) 571–581.
[24] J. Maxwell, A Treatise on Electricity and Magnetism, second ed. Oxford University Press, Cambridge, UK, 1904.
[25] S.V. Patankar, Numerical Heat Transfer and Fluid Flow, Hemisphere Publishing Corporation, Taylor and Francis Group, New York, 1980.
[26] G. De Vahl Davis, Natural convection of air in a square cavity, a benchmark numerical solution, Int. J. Numer. Meth. Fluid. 3 (1983) 249–264.